ELSEVIER

Journal of Alloys and Compounds 275–277 (1998) 384–387

Journal of ALLOYS AND COMPOUNDS

Crystal-field effects and simulation of the energy level scheme of Nd^{3+} in magnesium borate $MgNd(BO_2)_5$

C. Cascales[a,*], R. Sáez Puche[b], P. Porcher[c]

[a]*Instituto de Ciencia de Materiales de Madrid, CSIC, Cantoblanco, E-28049 Madrid, Spain*
[b]*Departamento de Química Inorgánica, Facultad de Ciencias Químicas, Universidad Complutense de Madrid, E-28040 Madrid, Spain*
[c]*Laboratoire de Chimie Métallurgique et Spectroscopie des Terres Rares, UPR 209 CNRS, 1, pl. A. Briand, F-92195 Meudon, France*

Abstract

Based on the energy level scheme of Nd^{3+} derived from the absorption spectra for $MgNd(BO_2)_5$, S.G. $P2_1/c$, at temperatures of 300, 77 and 9 K, a phenomenological parametrization of the free-ion and crystal-field effects was carried out. A descending symmetry method, from C_{2v} to C_2 symmetries, was used in the simulation of the configuration, leading to low r.m.s. deviation values. The crystal-field parameter sets are consistent with that corresponding to the same Eu^{3+}-doped borate matrix for each of these considered symmetries. Very good agreement of the observed crystal-field strength parameters is found when they are compared with the ab initio parameters calculated from crystal data for C_1, the real point symmetry of Nd^{3+} in the matrix. © 1998 Elsevier Science S.A.

Keywords: Absorption spectra; Phenomenological parametrization; Descending symmetry; Neodymium borate; Crystal field

1. Introduction

The well-known [1,2] structure of $RT(BO_2)_5$, R=rare earth, T=Mg, Co, Ni, consists of infinite sheets of $[BO_{10}]^{5-}$ composed of three sets of BO_4 tetrahedra and two types of BO_3 triangles joined by common corners, TO_6 distorted octahedra joined two by two sharing one common edge, and RO_{10} distorted polyhedra linked via common edges forming chains along the *b*-axis (Fig. 1). The crystallographic site of R^{3+} does not contain symmetry elements. Among these borates and due precisely to the one-dimensional character of the R–R interactions (R–R intrachain distance is ~4 Å, whereas the shortest R–R interchain distance is ~6.5 Å), the luminescence properties of rare earth magnesium borates $MgR(BO_2)_5$ have raised considerable interest [3–7]. In fact, very efficient phosphors can be obtained by using some codoped materials, such as, for example, with Ce^{3+} as the sensitizer, the Gd^{3+} sublattice as an intermediary and Tb^{3+} as the activator [7,8]. Finally, the crystal-field analysis of the $4f^6$ configuration of the Eu^{3+}-doped lanthanum magnesium borate

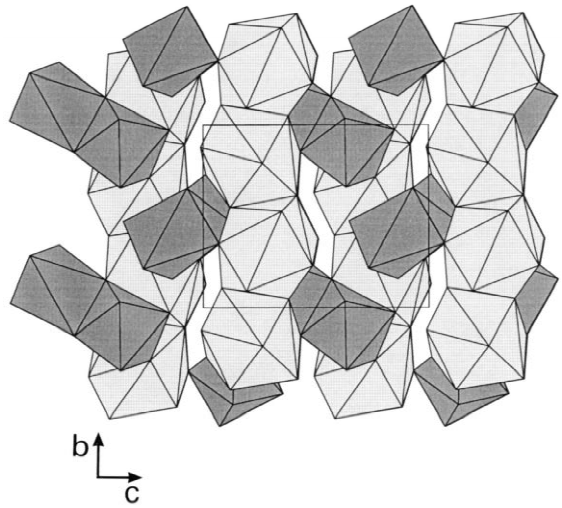

Fig. 1. Projection on the *bc* plane of the structure of $MgNd(BO_2)_5$ showing edge-sharing RO_{10} chains along *b*-axis and isolated $[Ni_2O_{10}]$ units.

*Corresponding author. Tel.: +34 1 3349027; fax: +34 1 3720623; e-mail: immcc53@fresno.csic.es

0925-8388/98/$19.00
PII: S0925-8388(98)00345-4

was made [9] using the observed $^7F_{JM}$ energy levels from the fluorescence spectrum.

The present work presents the results of the study of the absorption spectra, between 9 K and room temperature, for $MgNd(BO_2)_5$. From these data, the crystal-field analysis and the simulation of the Nd^{3+} energy level scheme were accomplished for the C_{2v} and then for the C_2 symmetries, for which either nine real, or nine real plus five complex crystal-field parameters (cfps) are involved, respectively. A comparison with the crystal-field strength parameters proceeding from a parallel ab initio calculation from crystal data, in this case considering the true C_1 symmetry of the Nd^{3+} position, is presented.

2. Experimental details

Polycrystalline $MgNd(BO_2)_5$ was prepared as described in the literature [9]. The absorption spectra were obtained on a Cary 2400 spectrometer, at temperatures of 300, 77 and 9 K. In order to compare with previous data [9], $LaMg(BO_2)_5$:Eu^{3+} was also synthesized and its fluorescence emission recorded at 300 and 77 K under the excitation of a CW argon ion laser and a dye laser adjusted on the $^5D_0$ level.

3. Simulation of the energy level scheme

The position of the discrete energy levels of the $4f^n$ configurations in solids is, in general well simulated using a Hamiltonian [10] which involves the adjustment of both free-ion and crystal-field parameters. The free-ion Hamiltonian considered here includes the spherically symmetric one-electron term of the Hamiltonian H_0, electrostatic parameters taking account the repulsion between equivalent f electrons, the magnetic spin–orbit interaction ζ_{4f}, two-body interaction terms through the Trees parameters α, β and γ, and three-body interaction terms parametrized with the Judd parameters T^k ($k=2$, 3, 4, 6, 7 and 8). Spin–spin, spin–other–orbit and other relativistic interactions of minor importance have not been included,

$$H_{FI} = H_0 + \sum_{k=0,1,2,3} E_k e^k + \zeta_{4f} A_{SO} + \alpha L(L+1) + \beta G(G_2) + \gamma G(R_7) + \sum_{k=2,3,4,6,7,8} T^k t_k \quad (1)$$

The crystal-field Hamiltonian is usually written in Wybourne's [11] formalism,

$$H = \sum B_q^k \cdot C_q^k \quad (2)$$

A few configurations ($4f^{1,2,3,11,12,13}$) can be treated without truncations, others ($4f^{6,7}$) have to be truncated, but, on the whole, coherent results are found for the values of the cfps of different lanthanides, utilized as crystal-field probes in the same site of isomorphous structures. The number of non-zero B_q^k and S_q^k cfps depends on the crystallographic site symmetry of the lanthanide ion. The serial expansion of the crystal-field potential corresponding to the very low C_1 point symmetry of R in the current case keeps non-zero all of the 27 cfps, which constituted nonrealistic conditions of simulation. Instead of C_1, the approximate C_2 (or C_s as well) point symmetry was used for the simulation involving 14 non-zero cfps, among which five complex cfps (S_2^2 is set to zero by an appropriate choice of the reference axis system). Moreover, for C_{2v} only the real part of the crystal-field Hamiltonian is considered, i.e. nine real B_q^k ($k=0$, 2, 4, 6; $q \leq k$) cfps. These approximations have been used previously [12,13].

Free-ion parameters for Nd^{3+} in various hosts are available in the literature and, in any case, they will not differ much from one environment to another. On the contrary, the cfps are different for different structures, although they should vary smoothly over an isostructural series. Thus, the process of simulation was started using free-ion parameters from Ref. [14] and the reported [9] phenomenological set of cfps corresponding to the same Eu^{3+}-doped matrix, which we previously tested with data from our own fluorescence measurements.

The laborious procedure to obtain the cfps will be facilitated if these starting values could be estimated by an ab initio calculation model. For this reason, and in order to compare with phenomenological values, the so-called simple overlap model, SOM, [15] was now applied. In fact, the authors have successfully used SOM over a wide variety of rare earth-containing matrices [16,17]. In this model the cfps are written as

$$B_q^k = \langle r^k \rangle \sum_\mu \rho_\mu \left(\frac{2}{1 \pm \rho} \right)^{k+1} A_q^k(\mu)$$

$$\rho = \rho_0 \left(\frac{R_0}{R} \right) \quad (2.5 < n < 5). \quad (3)$$

The sum runs over all ligands of the first coordination sphere, consequently required crystallographic data are restricted to the closest ligand positions, and $\langle r^k \rangle$ radial integrals [18] are not corrected from the spatial expansion. The overlap degree ρ in the wavefunctions associated to the bonding between the metal and the ligand varies for each ligand as a function of the distance from the central ion, and is referred to the closest ligand. A_q^k is the lattice sum, and it takes into account the symmetry properties of the metal site, including the effective charge attributed to the ligand. The sign $\pm$ of the denominator differentiates the type of ligand: when a single type of ligand is considered, a sign $-$, corresponding to the normal shift of the charge barycenter from the middle of the bonding distance should be taken, and when different ligands are present the sign $-$ corresponds to the most covalent.

Comparisons between experimental and ab initio SOM

cfps, for the true C_1 symmetry, were made through the corresponding crystal-field strengths S_k, for the cfps of rank k, and the total crystal-field strength, S [19],

$$S_k = \left\{ \sum_k 1/(2k+1) \left[(B_0^{k^2}) + 2\sum_{kq} [(B_q^k)^2 + (S_q^k)^2] \right] \right\}^{1/2}, S = \left[\frac{1}{3} \sum_k S_k^2 \right]^{1/2} \quad (4)$$

In these comparisons the three adjustable parameters required for the model were fixed to the typical values of 3.5, −0.8 and 0.07, for n, the effective charge for oxygen, and the overlap ρ, respectively.

The simulations were performed by the programs REEL and IMAGE (P. Porcher, FORTRAN routines REEL and IMAGE for simulation of d^n and f^n configurations involving real and complex crystal-field parameters, 1989, unpublished data). Crystallographic data were taken from Ref. [2].

4. Results and discussion

Transitions in the absorption spectrum of Nd^{3+} at 9 K originate from the lowest level of the $^4I_{9/2}$ manifold. Therefore the positions of the excited states can be directly established from these measurements. The positions of the crystal-field components of $^4I_{9/2}$ have been established from transitions to $^2P_{1/2}$ at room temperature. Thus, an energy level scheme of 69 levels was determined despite the vibronic structure of the electronic spectra of Nd^{3+} in the studied matrix. Parts of this spectrum are presented in Fig. 2a,b. Throughout the refinement process the γ parameter was fixed to a standard value since the levels in which its effect is really of importance are not experimentally observed ($^2F(2)$ terms, for instance). Moreover, for the same reason T^2 and T^8 could not be varied freely. In no case were large individual discrepancies between experimental and calculated energy levels detected. In contrast with reported results in the Eu^{3+} configuration [9], an improvement in the reproduction of the energy levels is achieved for the C_s symmetry, the rms deviations assuming a lower value and the complex parameters getting fixed to stable values different from zero.

Table 1 also compares cfps for the Eu^{3+}-doped compound, those reported previously and a newly obtained set together. The similarity of the Eu^{3+} and Nd^{3+} parameter sets supports the unique nature of the simulation, and moreover it is an indication of its consistence.

Ab initio SOM cpfs have been calculated for C_1, the true symmetry for the Nd^{3+} site, and in this case the crystal-field potential involves a large number of cfps, 27, far away of that experimentally obtained. Thus, in order to compare them, the use of their corresponding crystal-field strength parameters is a more reasonable approach. Table 2 includes crystal-field strength parameters for $MgNd(BO_2)_5$ from both spectroscopic and ab initio SOM calculation. S_k

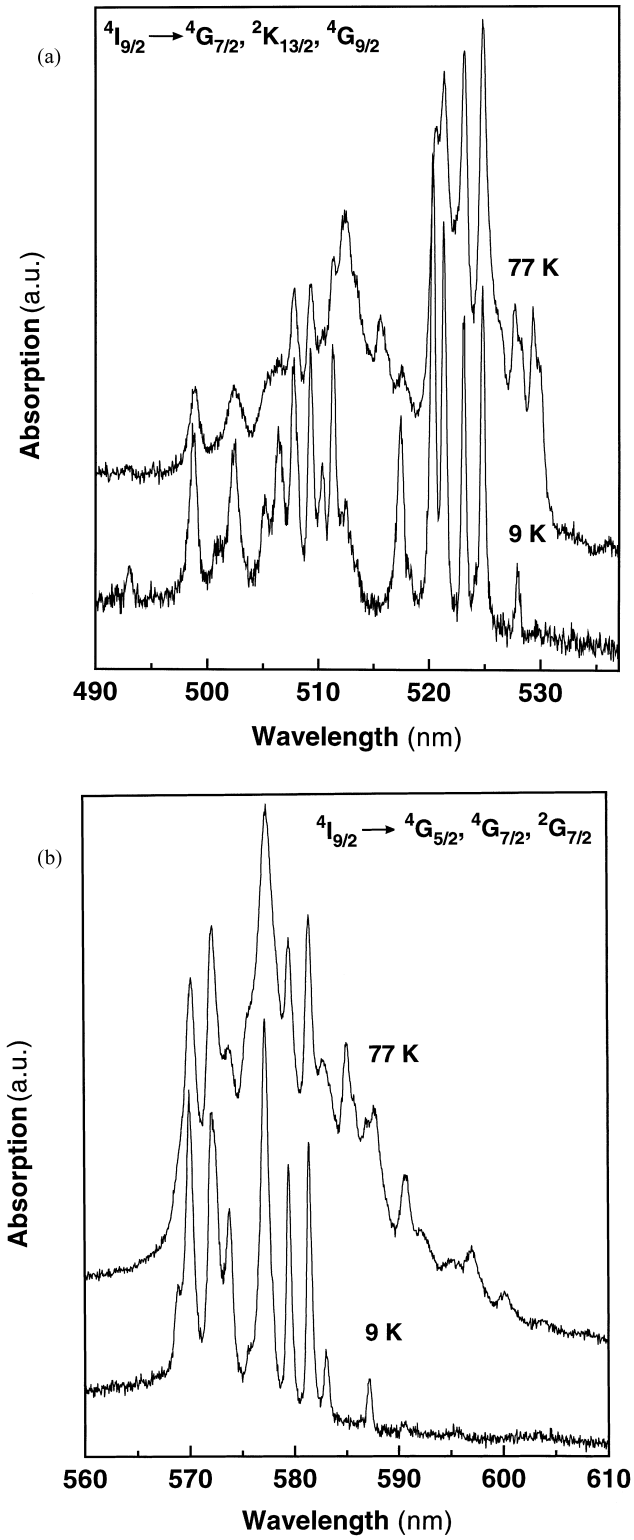

Fig. 2. (a,b) Comparison of parts of the absorption spectra of $MgNd(BO_2)_5$ at 77 and 9 K.

SOM values are slightly underestimated when compared to the experimental ones, although in the worst case, S_6, the calculation reproduces the experiment with a precision better than 85%. The most evident reason for this be-

Table 1
Free-ion and crystal-field parameters for Nd^{3+} in $MgNd(BO_2)_5$

	Nd		Eu	
	C_{2v}	C_2	C_{2v}	C^a_{2v}
E^0	23 866 (2)	23 843 (1)		
E^1	4983 (1)	4932 (1)		
E^2	24.35 (2)	23.52(2)		
E^3	483.8 (2)	483.0 (1)		
α	21.10 (5)	18.62 (5)		
β	−557 (4)	−500 (4)		
γ	[750]	[750]		
ζ	871.5 (9)	869.8 (8)		
T^2	[355]	[355]		
T^3	24 (2)	23 (2)		
T^4	114 (3)	97 (3)		
T^6	−204 (8)	−238 (8)		
T^7	295 (15)	305 (11)		
T^8	[311]	[311]		
B^2_0	1023 (15)	987 (16)	1074 (17)	1072
B^2_2	264 (13)	314 (16)	255 (19)	250
B^4_0	1126 (34)	1068 (38)	632 (36)	657
B^4_2	−418 (38)	−263 (47)	−333 (26)	−314
S^4_2		−452 (45)		
B^4_4	−30 (33)	300 (57)	−377 (36)	−314
S^4_4		−50 (40)		
B^6_0	1222 (52)	1186 (50)	1080 (36)	1158
B^6_2	915 (54)	826 (47)	521 (33)	486
S^6_2		265 (78)		
B^6_4	−568 (44)	−49 (89)	−540 (30)	−599
S^6_4		−534 (62)		
B^6_6	673 (45)	−383 (82)	481 (34)	411
S^6_6		646 (55)		
Levels	69	69	18	34
σ	16.4	14.8	6.9	7.1
S	16229	12054	427	435

The values in square brackets indicate parameter not varied. The values in parentheses refer to estimated standard deviations. For comparison, crystal-field parameters for Eu^{3+} are added. All values are in cm^{-1} units. [a]See Ref. [9].

haviour arises from the fact that the crystallographic structure in which SOM is based has been determined at room temperature, whereas the energy level scheme is mainly deduced from liquid helium temperature measurements. This feature can limit the comparison because in some cases a small variation of the metal–ligand distance can induce a strong variation in the cfps values. Apart from this, both sets have very comparable orders of magnitude.

As a conclusion, we think that SOM offers a good opportunity for estimating cfps from the crystalline structure, this kind of calculation being of particular interest when opaque materials are to be considered.

Table 2
Comparison between observed and SOM-calculated crystal-field strength parameters for Nd^{3+} in $MgNd(BO_2)_5$

S_k	C_{2v}	C_2	SOM C_1
S_2	472	463	443
S_4	400	409	364
S_6	489	476	420
S_T	455	450	410

All values are in cm^{-1} units.

Acknowledgements

One of the authors (C.C.) acknowledges the financial support from the ‘Domingo Martínez’ Foundation.

References

[1] B. Saubat, M. Vlasse, C. Fouassier, J. Solid State Chem. 34 (1980) 271.
[2] J.A. Campá, C. Cascales, E. Gutiérrez Puebla, J. Mira, M.A. Monge, I. Rasines, J. Rivas, C. Ruíz Valero, J. Alloys Compounds 225 (1995) 225.
[3] B. Saubat, C. Fouassier, P. Hagenmuller, J.C. Bourcet, Mater. Res. Bull. 16 (1981) 193.
[4] C. Fouassier, B. Saubat, P. Hagenmuller, J. Lumin. 23 (1981) 405.
[5] M. Saakes, G. Blasse, Phys. Stat. Sol. 78 (1983) K97.
[6] M. Saakes, M. Leskelä, G. Blasse, Mater. Res. Bull. 19 (1984) 83.
[7] M. Leskelä, M. Saakes, G. Blasse, Mater. Res. Bull. 19 (1984) 151.
[8] J.Th.W. de Hair, J.T.C. van Kemenade, 3rd Int. Conf. Sci. Tech. Light Sources, Toulouse, France, 1983.
[9] J. Hölsä, M. Leskelä, Mol. Phys. 54 (1985) 657.
[10] W.T. Carnall, G.L. Goodman, K. Rajnak, R.S. Rana, J. Chem. Phys. 90 (1989) 3443.
[11] B.G. Wybourne, Spectroscopic Properties of Rare Earths, Wiley, New York, 1965.
[12] C. Cascales, E. Antic Fidancev, M. Lemaitre Blaise, P. Porcher, J. Alloys Compounds 180 (1992) 111.
[13] C. Cascales, E. Antic Fidancev, M. Lemaitre Blaise, P. Porcher, J. Phys.: Condens. Matter 4 (1992) 2721.
[14] E. Antic Fidancev, C. Cascales, M. Lemaitre Blaise, P. Porcher, J. Alloys Compounds 207–208 (1994) 178.
[15] O.L. Malta, Chem. Phys. Lett. 88 (1982) 353.
[16] C. Cascales, P. Porcher, R. Sáez Puche, J. Phys.: Cond. Matter 8 (1996) 6413.
[17] C. Cascales, P. Porcher, R. Sáez Puche, J. Alloys Compounds 250 (1997) 391.
[18] A.J. Freeman, J.P. Desclaux, J. Magn. Magn. Mater. 12 (1979) 11.
[19] N.C. Chang, J.B. Gruber, P.R. Leavitt, C.A. Morrison, J. Chem. Phys. 76 (1982) 3877.